Effects of frustration on the spin dynamics of the zigzag honeycomb lattice

E. M. Wilson and J. T. Haraldsen

Department of Physics, University of North Florida, Jacksonville, Florida 32224, USA

and Materials Science and Engineering Program, University of North Florida, Jacksonville, Florida 32224, USA

This investigation covers the effects of variable exchange interactions on the spin dynamics of the zigzag honeycomb lattice. Using a Holstein-Primakoff expansion of the Heisenberg Hamiltonian with easy-axis anisotropy, we characterize the effects of multiple nearest-neighbor (NN) and next-nearest-neighbor (NNN) interactions with asymmetry within the context of a frustrated and nonfrustrated zigzag magnetic configuration. By building the model term by term, we directly observe the behavioral contributions from each interaction, how the system changes with anisotropy, and how asymmetric terms transform the system from a nonfrustrated to a frustrated state. By analyzing geometric frustration, we are able to demonstrate the role that NN and NNN interactions play within an asymmetric honeycomb lattice, show the emergence of direction-dependent Dirac nodes, and postulate that the standard Heisenberg interaction has a notable contribution to the behavior observed in the spin excitation behavior within the high-symmetry pathway Γ-M. Furthermore, to examine the efficacy of our model, we compare it to known inelastic neutron scattering data for α-RuCl$_3$, which has been established to host a zigzag honeycomb ground state dominated by anisotropic interactions.

I. INTRODUCTION

The dramatic increase in the use of electronic devices in all aspects of the world has fueled a great need for high-efficiency materials. As the electronic demand increases with faster data consumption, cryptocurrency, and high-speed internet use, the energy demand and carbon footprint for electronics put them in the spotlight [1–3]. In pursuing more energy-efficient electronics, the best way to improve devices is to have better materials that provide the same or better ability to store and transfer information as current electronic devices [4,5].

Areas of interest that have gained attention in the past few decades are the fields of spintronics and magnonics, which manipulate the properties of spin and spin waves for information transport [6,7]. Since magnetic interactions (∼1– 10 meV) are typically smaller than electronic excitations (∼1 eV), spintronic and magnonic devices have the potential to provide considerable energy savings while maintaining or even exceeding the speed and fidelity of standard electronic components [8–10].

To identify materials that allow for the utilization of magnons and spin waves for application purposes, it is crucial to understand how magnetic interactions affect the propagation of spin excitations through various lattice configurations [11]. Previous studies have provided insight into square, hexagonal, honeycomb, and Kagome lattices [12–14]. Each lattice configuration has various magnetic configurations consisting of ferromagnetic and antiferromagnetic interactions. The honeycomb and kagome lattices are particularly interesting due to the multiple sublattice interactions that can lead to Dirac nodes and potential exotic spin states like the elusive quantum spin liquid [15–17].

Since the discovery of graphene [8,18], the interest in two-dimensional systems has been promulgated due to the fascinating nature of graphene's properties and potential applications. Like such, many new two-dimensional materials have fallen under investigation and the production of multiple honeycomb systems with similar properties has come to light, such as Na$_2$IrO$_3$, RuCl$_3$, CrX_3 (X = Cl, Br, and I), and more [16,19–22]. With the two-dimensional honeycomb lattice on the rise, we take a deeper look into the generalized honeycomb's magnetic structure and how the magnetic interactions respond to outside perturbation.

As shown in Fig. 1(a), the honeycomb lattice is a special form of hexagonal lattice that consists of two sublattices, where the primitive translation vectors of the hexagonal lattice introduce angles of 120° in between equal lengths and rotate 90° with length $b = 4\pi/a\sqrt{3}$ within reciprocal space. Within the context of spin exchange, such a structure can present five different collinear (and other noncollinear) magnetic structures such as ferromagnetic (FM), antiferromagnetic (AFM), zigzag (ZZ), dimerized (DIM), and armchair (ARM) [13,23]; however, the focus of this study is on the zigzag magnetic configuration.

In this study, we focus on the ZZ AFM configuration of the honeycomb lattice and use a Heisenberg spin Hamiltonian to investigate the effects of nonfrustrated and frustrated interactions on the spin-wave excitations. Through a Holstein-Primakoff expansion with easy-axis anisotropy, we effectively characterize the effects of multiple nearest-neighbor and next-nearest-neighbor interactions and of asymmetry within the context of a frustrated and a nonfrustrated zigzag magnetic configuration. To begin understanding the zigzag magnetic configuration and how the spin waves are affected by competing interactions, it is necessary to note the behavior shown in the most basic FM and AFM configurations.

It is observed that the introduction of spin into the honeycomb lattice complicates the presence of inversion symmetry in the two-sublattice structures [13]. Observing the FM configuration, it is seen that, in every direction, inversion symmetry is maintained and, therefore, should produce a Dirac
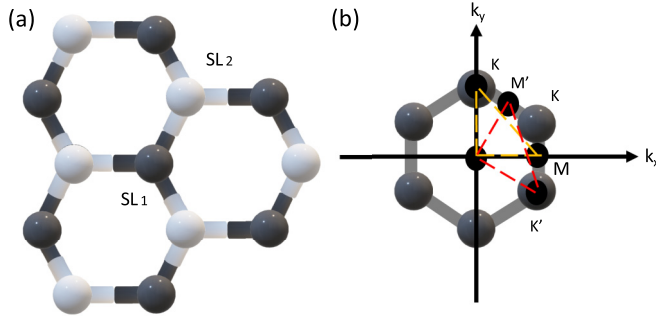
FIG. 1. (a) An illustration showing the physical configuration of the honeycomb lattice as a two-sublattice hexagonal structure. (b) The reciprocal space representation of the honeycomb lattice and the high-symmetry-pathways Γ-M-K-Γ-M′-K′-Γ.

cone [17]. Interestingly, in the AFM configuration, no matter what direction is analyzed, when the magnetic structure is imposed, it is found that inversion symmetry is broken and produces only a single-band mode within its spin-wave spectra [13,16,23,24].

II. ZIGZAG SPIN HAMILTONIAN

The zigzag magnetic configuration, characterized by a collinear arrangement of spins, demonstrates a unique pattern where nearest-neighbor and next-nearest-neighbor atoms interact along a distinctive "zigzag" path (see Fig. 2). This striking configuration dynamically oscillates between FM and AFM interactions. Intriguingly, within the framework of the zigzag magnetic arrangement, a noteworthy phenomenon
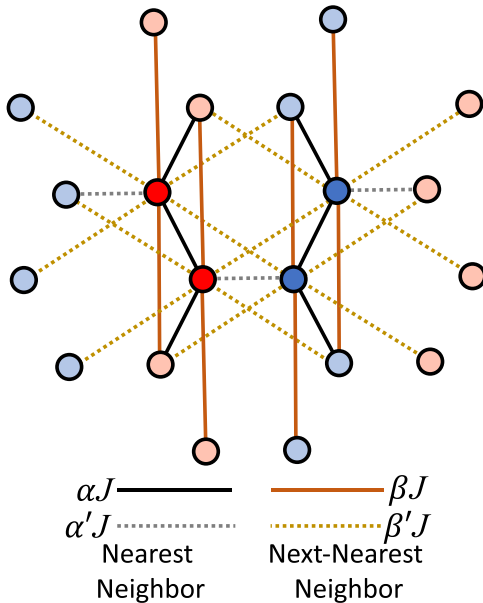

FIG. 2. Four-sublattice interactions where α is the nearest-neighbor interaction and β is the next-nearest-neighbor interaction. The prime terms α' and β' are asymmetric nearest-neighbor and next-nearest-neighbor interactions, respectively. The blue lattice sites represent the up spin, the red lattice sites represent the down spin, and the darker red/blue sites represent the unit cell.

emerges: when observed in a specific direction, inversion symmetry is preserved. Moreover, inversion symmetry remains preserved along two distinct directions upon system rotation. This observation holds the potential to uncover the existence of magnetic Dirac nodes [25–28]. The effective Hamiltonian for this model, then, is

$$
H = -\frac{J}{2}\Bigg[\sum_{\mathrm{NN}} \alpha \vec{S}_i \cdot \vec{S}_j + \sum_{\mathrm{NNN}} \beta \vec{S}_i \cdot \vec{S}_j
$$
$$
+ \sum_{\mathrm{nn}} \alpha' \vec{S}_i \cdot \vec{S}_j + \sum_{\mathrm{nnn}} \beta' \vec{S}_i \cdot \vec{S}_j \Bigg] - D \sum_i S_{iz}^2. \quad (1)
$$

The terms involving $\alpha = J_1/J$, $\alpha' = J_1'/J$, $\beta = J_2/J$, and $\beta' = J_2'/J$ correspond to the nearest-neighbor (NN and nn) and next-nearest-neighbor (NNN and nnn) interactions, respectively. NN and NNN interactions are between like spins and nn and nnn interactions are between opposite spins. The final term represents the single-ion anisotropy, D, associated with each spin site i. The positive scaling factors correspond to ferromagnetic interactions, while negative ones indicate antiferromagnetic interactions. This comprehensive Hamiltonian captures the intricate interplay between exchange interactions and anisotropy, crucial for understanding the magnetic properties of the system; however, an expansion of the terms is still necessary for capturing the dispersion relation of spin-wave excitation within a bosonic system [29].

To determine the spin-wave dynamics, a Holstein-Primakoff (HP) expansion is employed on the Heisenberg spin Hamiltonian, allowing us to delve into the effects of nearest-neighbor and next-nearest-neighbor interactions [26,28]. The HP transformation involves mapping the spin operators onto these bosonic operators and then truncating the expansion at certain orders in $1/S$ [29–31]. The HP transformation enables us to express the spin operators as combinations of bosonic creation ($b_i^\dagger$) and annihilation (b_i) operators, which correspond to magnons, the quanta of spin excitations. Utilizing the known region of stability for the ZZ magnetic phase [13], we use an exact diagonalization of the spin dynamics matrix, which is composed of exchange interactions and produces the observed magnon modes [32–34]. By building the model by its components, we look to provide insight into how each interaction affects the total behavior and its role in the spin dynamics of a ZZ magnetic structure. By analyzing these parts individually, insight into the interactions and how they affect the resultant perturbation is prevalent.

A. Effects of nearest and next-nearest neighbors

To show the evolution of the spin dynamics represented by a ZZ magnetic configuration within a honeycomb lattice, we start with a base case where the nearest-neighbor interaction $\alpha > 0$, and all other interactions are set to 0. In this regime, the zigzag configuration consists of decoupled ferromagnetic ZZ stripes of up and down spins in the honeycomb lattice that are mirror images of each other. α needs to be ferromagnetic along the ZZ direction as it stabilizes the spin wave. A negative α in this case would lead to an instability in the spin-wave spectra as the ZZ configuration requires parallel spins. As shown in Fig. 3(a), there are two spin waves produced
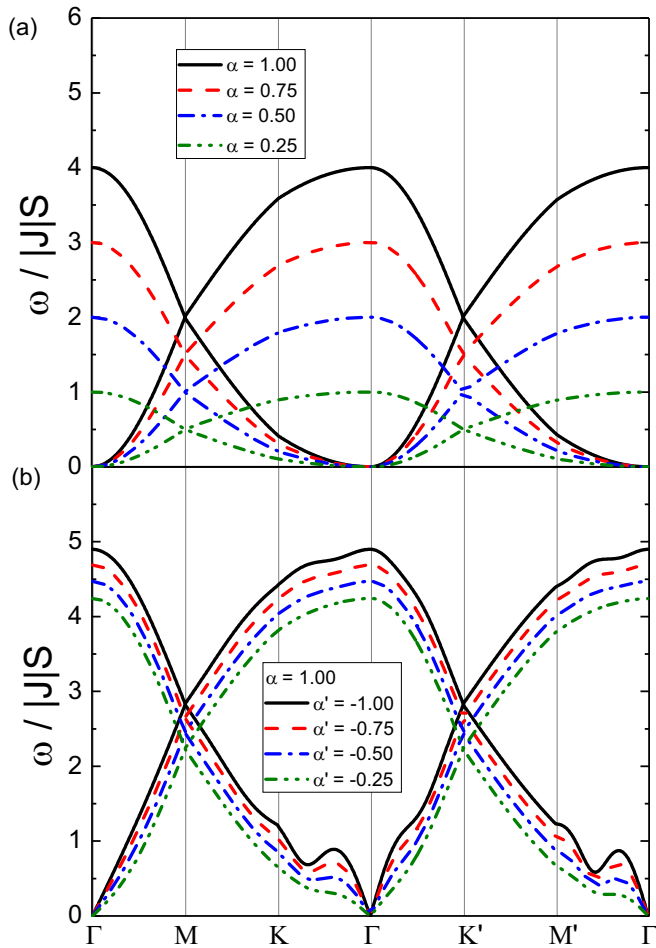
FIG. 3. (a) Two-dimensional plot showing the nearest-neighbor interaction's behavior as α is added. This produces two direction-dependent diagonal nodes at M and K'. Panel (b) shows how this changes as deformities are introduced as α'. This creates distortions in the spin wave that increase alongside α'.

FIG. 4. (a) Two-dimensional plot showing the next-nearest-neighbor interaction's behavior as β is added. Panel (b) shows how this changes as deformities are introduced as β'. This creates distortions in the spin wave and increases alongside β'. Only one spin wave is produced as the interactions of the next-nearest neighbor degenerate in this direction.

due to the two opposing zigzag chains. As α increases, the energy dispersion is scaled by α along the high-symmetry pathway Γ to M to K and back to Γ. The resultant spin wave progresses from a smooth behavior to a more deformed propagation, most noticeably from M to K', as the magnitude of α increases. Observably, the symmetry of the ZZ chains produces two spin-wave modes with distinct crossing points between the two spin-wave modes arising at high-symmetry points M and K'. This crossover indicates the potential for Dirac magnons similar to those observed in the FM magnetic phase [13,16]. However, considering only the NN interaction, these crossover points are produced by two decoupled spin waves with inversion symmetry, which increases the potential for Dirac magnons [15].

Furthering our investigation of the ZZ magnetic configuration, the ferromagnetic chains are coupled with the nearest-neighbor interaction α', which produces an asymmetry relative to α. As $\alpha = 1.00$ remains ferromagnetic, the natural, nonfrustrated order is to introduce α' to be antiferromagnetic since the ZZ magnetic order is not stable without anisotropy when $\alpha = \alpha'$. This configuration provides insight
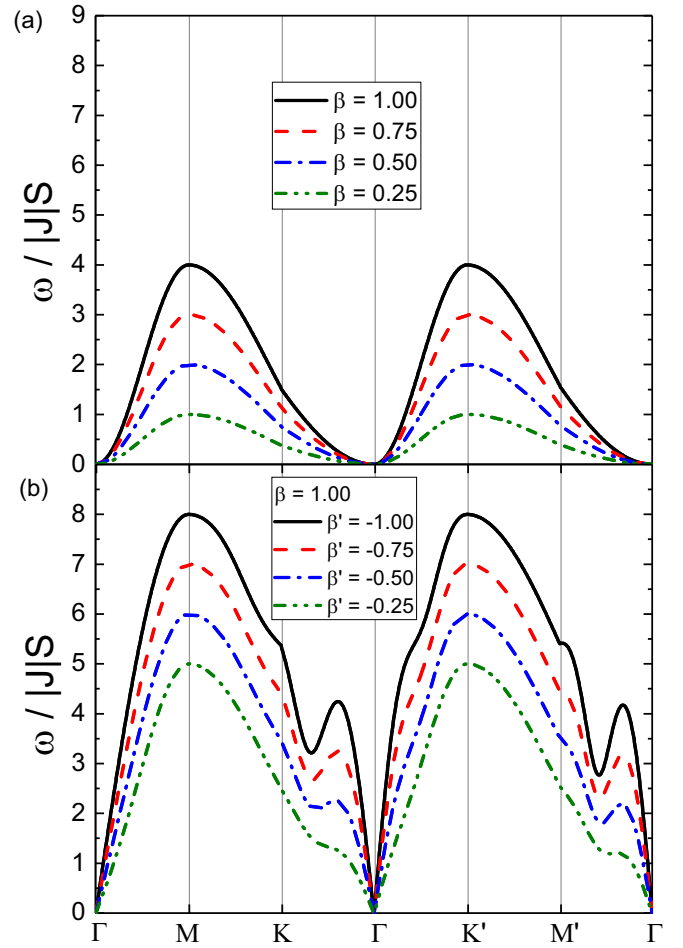
into the role α' plays within the model and how it affects the behavior reflected in the first case where there was no α'.

Starting with $|\alpha| > |\alpha'|$, small values of α' are added and steadily increased until $\alpha' = -\alpha$. As the values increase, the noted deformities in Fig. 3(b) become profound, and new distinct behavior blatantly presents itself from K to Γ' and M' to Γ. It is observed that the stability increases with the introduction of α' as the high-symmetry points become more recognizable, and the spin-wave velocity shifts from being quadratic in behavior to linear. As α' increases, the spin waves produced within the Brillouin zone have a higher dispersion energy due to the increase in the energy of the system.

Continuing with the same method, the next-nearest-neighbor interaction is examined by itself with $\beta > 0$, and all other interactions are set to 0. As shown in Fig. 4(a), the resultant spin wave has only one mode, which is due to the ferromagnetic chains being identical, which produces the emergence of a singular mode. The modes mentioned above are stable and demonstrate the same scaling of the spin wave that was observed with nearest-neighbor interactions as β
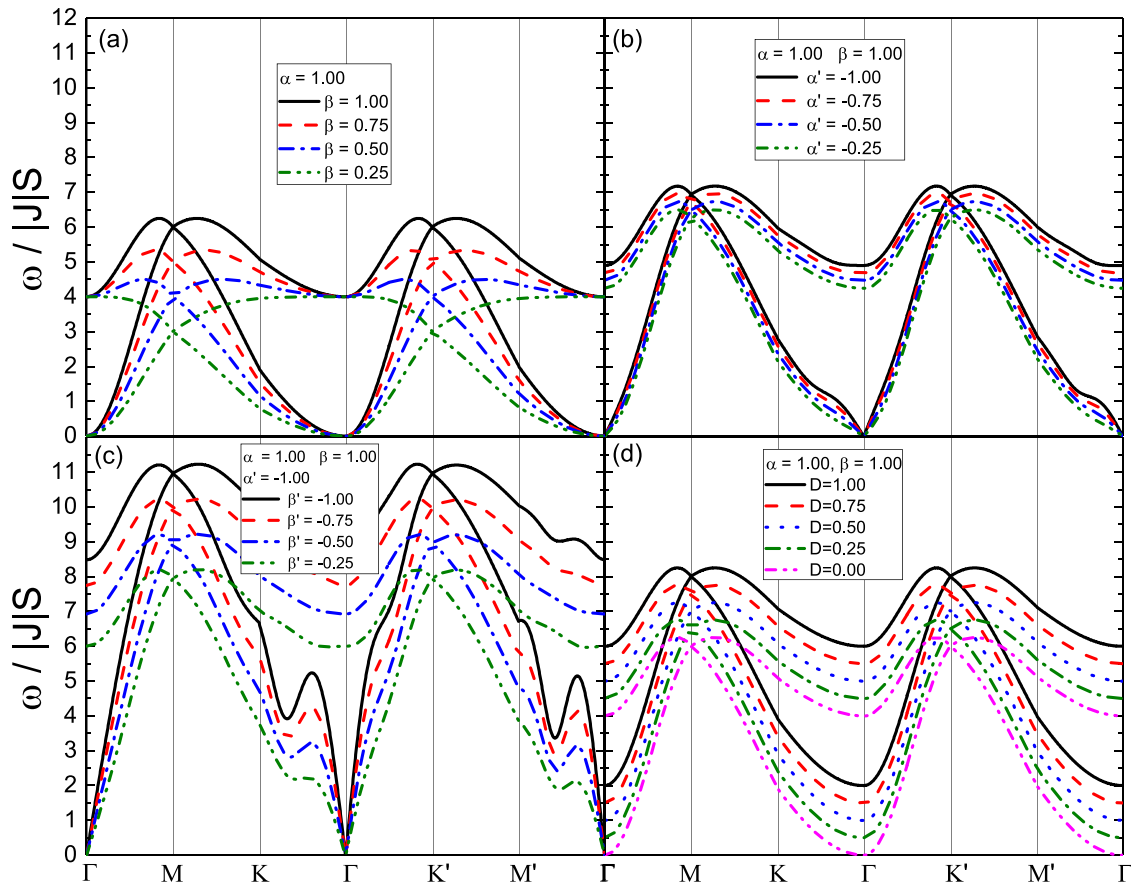
FIG. 5. Two-dimensional plot of the evolution of spin waves within the nonfrustrated model as the interactions change. Each plot starts dotted and becomes more solid with each increment until the final calculation, which is the solid black. Starting in panel (a) with $\alpha = -1.00$, β is added in increments of -0.25 until it reaches $\beta = -1.00$. In panel (b), α' produces deformities and is added similarly. This adds small changes in the behavior but not much energy. As β' is introduced in panel (c), the changes in the spin wave become more accented, and the deformities become more prevalent with higher energies. An anisotropy test in panel (d) shows how it affects the calculations. As anisotropy is added, the energy of the spin wave increases all around without changing the behavior.

increased. The change for the next-nearest-neighbor interaction is reflected in Fig. 4(a), where the dispersion invoked by the next-nearest-neighbor interaction is double degenerate and would explain the interaction not changing for its spin.

Similarly to the case where the nearest-neighbor interaction was examined, asymmetry is added to the system by introducing β', which produces decoupled triangular lattices. Setting $\beta > 0$ increases asymmetry and starts to add distinct behavior to the interaction. As with the introduction of α', the spin-wave velocity shifts from quadratic to linear as the dispersion energy approaches 0 at Γ from both K and M′ [shown in Fig. 4(b)]. Seemingly, the next-nearest-neighbor interaction has strong effects on systems such as the AFM configuration and, therefore, could play a dominant role in the ZZ magnetic configuration due to the double degeneracy. Determining the evolution of a zigzag magnetic configuration's spin dynamics in a honeycomb lattice depends on all the constituent parts.

B. Nonfrustrated model

Within the nonfrustrated model, all the interactions coalesce without competition where they are "content" in their configuration. Starting at the nearest-neighbor interaction α,

a next-nearest-neighbor interaction β is added. Observing how the response to disturbance changes with the addition of another interaction, the nearest-neighbor interaction is set to a FM interaction $\alpha = 1.00$. The FM next-nearest-neighbor interaction β is then added in increments of 0.25 until $\alpha = \beta$. Figure 5(a) illustrates the calculations as the interactions approach being equal, starting as a dashed line and progressing to a solid line with the increase of β. The overall energy spectrum increases at the peaks M and K′, and the troughs at Γ drop in energy and become more defined, which suggests that, between the two, the nearest-neighbor interaction dictates the behavior observed, and the addition of the next-nearest-neighbor increases the strength of the spin wave and controls the presented crossover points. This effect is potentially due to the degeneracy presented in Fig. 4, where all the spin waves have the same energy levels, and only one perturbation is preserved. The produced spin wave by α is then shaped by the degeneracy that is introduced by β. The crossover points are presented on the high-symmetry locations M and K′ at $\frac{\omega}{|J|S} \approx 6$ as $\alpha = \beta$.

Figure 5(b) continues with $\alpha = \beta$; a second nearest-neighbor interaction called α' is added and is set to be AFM. As α' increases by increments of -0.25 until $\alpha' = -1.00$,

the general characteristics of the spin wave do not change. Instead, what is observed is a small gradual increase in the asymmetry as the behavior itself becomes more defined and the overall energy increases. Moreover, deformities begin to present themselves from K-Γ and M′ − Γ, but only slightly. These deformities are expected due to the competition between interactions, which is consistent with the introduction of $α'$ to $α$ in Fig. 3(b).

Furthermore, in Fig. 5(c) the nonfrustrated model is completed by the addition of asymmetry among the next-nearest-neighbor interactions with $β'$. The calculations are continued by starting with $α = β = −α'$ and adding $β'$ in increments of −0.25. The deformations presented from K to Γ and M to Γ by adding $α'$ become very distinct as the energy increases across the spin wave. With all interactions $α = β = −α' = −β'$ represented in the solid black line in Fig. 5(c), the crossover points are observed to shift up to $\frac{ω}{|J|S} ≈ 11$, and the system continues to be stable.

The nonfrustrated model does not require easy-axis anisotropy as all the nearest-neighbor and next-nearest neighbors match their configuration within the honeycomb lattice. In Fig. 5(d), anisotropy is added similarly to the other calculations by adding increments of 0.25 to the initial case of $α = β = 1.00$. As the single-ion anisotropy increases, the energy is proportionally increased across the spin wave without changing the observed propagation. Seemingly, the system's response to an outside disturbance within a nonfrustrated model is stable without requiring any anisotropy.

Investigating the nonfrustrated model highlighted how interactions seamlessly merged without competition, maintaining a harmonious "content" configuration. Starting with the nearest-neighbor interaction $α$, we introduced the next-nearest-neighbor interaction $β$. As $β$ gradually approached equality with $α$, the reflected changes unveiled an overall energy spectrum increase at peaks M and K′, while troughs at Γ became more defined. This emphasized the dominance of the nearest-neighbor interaction dictating the observed behavior, with the next-nearest neighbor enhancing the spin-wave strength and controlling crossover points, potentially due to the effect degeneracy introduces observed in Fig. 4.

Continuing the exploration by introducing an AFM second nearest-neighbor interaction $α'$ when $α = β$ revealed a gradual increase in asymmetry and defined behavioral changes, evident from K-Γ and M′ − Γ, aligning with prior observations in Fig. 3. Further completion of the nonfrustrated model with asymmetry among the next-nearest-neighbor interactions $β'$ exhibited distinct deformations across the spin wave as energy increased to $\frac{ω}{|J|S} ≈ 11$, maintaining stability without requiring easy-axis anisotropy.

C. Frustrated model

The honeycomb lattice is characterized by a coordination number of three and bipartite properties. Its sites can be partitioned into two sublattices, where each site within one sublattice exclusively connects to sites in the other sublattice [35]. Geometric frustration emerges as the lattice's triangular arrangement conflicts with the magnetic interactions among its components. This results in frustration, where the concurrent minimization of all interactions becomes unattainable [36,37]. This phenomenon is frequently encountered in systems featuring specific lattice symmetries, such as triangular or honeycomb lattices, and it gives rise to exotic phenomena like spin-ice and spin-liquid phases [12,25,29].

A honeycomb system with identical magnetic interactions does not match the physical configuration and forces a competition of exchange interactions. As the interactions vie to be stable within their configuration, frustration is produced within the system, causing a different dispersion. Figure 6(a) shows the nonfrustrated model where $α$ and $β$ are AFM and $β$ is introduced in increments of −0.25. When $α = β$, a different AFM nearest-neighbor interaction is introduced as $α'$, breaking the symmetry within the nearest-neighbor interactions, which causes the dispersion to become completely unstable until easy axis anisotropy (D) is instituted and stabilizes the interactions at $D = 3.10$. The introduction of asymmetry produces an inversion of the behavior presented in the nonfrustrated model, dropping the crossover point of the spin wave from $\frac{ω}{|J|S} ≈ 6$ to ≈0.8 as observed in Fig. 6(b). As $α'$ is increased by −0.25, the behavior remains the same, and the energy makes a small shift from $\frac{ω}{|J|S} ≈ 6.5$ up through to $\frac{ω}{|J|S} ≈ 7.2$, but the Dirac node remains the same.

Continuing the trend of adding asymmetry, next-nearest-neighbor asymmetry is initiated as $β'$. This causes the energy to shift up to $\frac{ω}{|J|S} ≈ 8$, and as $β'$ increases, the required anisotropy to stabilize the system decreases. Moreover, by increasing the next-nearest-neighbor asymmetry, the peaks of the dispersion begin to collapse, creating smaller peaks between M-K-Γ-K′ and from M′ − Γ as can be seen in Fig. 6(c). To further understand the dynamics between the frustration in the interactions, a variation of how the asymmetry is introduced is established by beginning with the next-nearest-neighbor asymmetry and bringing in the nearest-neighbor asymmetry in increments of −0.25. The deformation of the spin waves is initially present, and as $α'$ increases, the anisotropy decreases, and the peaks between M-K-Γ-K′ and from M′ − Γ become more defined in Fig. 6(d).

Overall, in the frustrated model, we observed a scenario where identical magnetic interactions led to competitive behavior produced by next-nearest-neighbor interaction that induces frustration and results in a distinctive dispersion. Introducing AFM $α'$ disrupted symmetry, leading to an unstable dispersion until stabilized by the imposition of easy-axis anisotropy. This alteration caused a significant shift in the crossover point from $\frac{ω}{|J|S} ≈ 6$ to $\frac{ω}{|J|S} ≈ 0.8$, showcasing a remarkable inversion in the behavior of the spin wave. The addition of further asymmetry, especially with the introduction of $β'$, demonstrated shifts in energy up to $\frac{ω}{|J|S} ≈ 8$, concurrently decreasing the required anisotropy for system stabilization. We then examined variations in asymmetry, initiating next-nearest-neighbor asymmetry $β'$ and systematically introducing nearest-neighbor asymmetry $α'$. These analyses uncovered initial deformations in the spin waves, accompanied by a decrease in anisotropy as $α'$ increased; this process yielded refined peaks observed between M-K-Γ-K′ and from M′ − Γ, offering comprehensive insights into the intricate dynamics underlying the frustration within interactions.
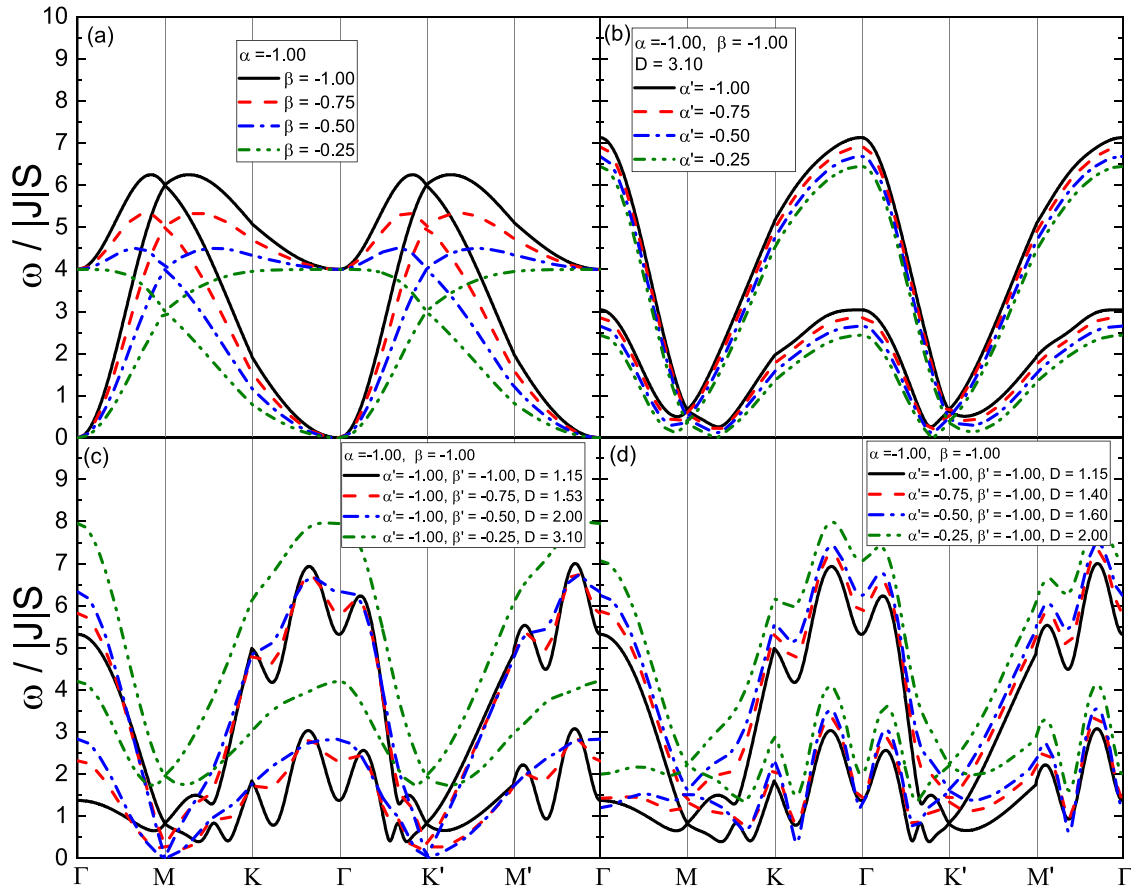
FIG. 6. Two-dimensional plot of the evolution of spin waves within the frustrated model as the interactions change. Each plot starts dotted and becomes more solid with each increment until the final calculation, which is the solid black. Starting in panel (a) with the nonfrustrated model, α is set to -1.00, and β is added in increments of -0.25 until it reaches $\beta = -1.00$. After this, we add competition of exchanges through α' in panel (b). This is done in similar increments and requires anisotropy to stabilize the behavior. This also causes the Dirac nodes to drop in energy, and the overall behavior of the spin wave inverts. β' is introduced, increased in panel (c), and adjusted in different ratios in panel (d). As β' is added, the anisotropy to stabilize the system is reduced and defines the deformities that appear in the spin wave.

III. FRUSTRATED MODEL APPLIED TO α-RuCl$_3$

Building upon the insights gained from our investigation into frustrated magnetic systems on a zigzag honeycomb lattice, we apply our easy-axis frustrated model to a current material of interest in the condensed-matter community [38,39]. α-RuCl$_3$ is composed of thinly interconnected layers of RuCl$_6$ octahedra that share edges, with the central Ru^{3+} ions with $4d^5$ orbital arranged in an almost perfect honeycomb configuration, a critical factor utilized in the Kitaev-Heisenberg model [40]. This indicates α-RuCl$_3$ as a prime candidate for the realization of fractionalized Kitaev physics, as well as quantum spin-liquid behavior [41–44].

Considering that Ru^{3+} ions carry a spin of $S = 1/2$, a honeycomb arrangement allows for the possibility of frustration between the Ru-Ru bonds in a single crystal. The magnetic moments of the Ru ions align antiparallel to each other along one direction and then reverse their alignment along the perpendicular direction, which results in a zigzag pattern of magnetic moments in the material [21,29,39,45]. Given the honeycomb's propensity to induce frustration in magnetic configurations, the interactions become highly anisotropic and

depend on the spins relative to the bonds between Ru^{3+} ions [35,39].

To understand the α-RuCl$_3$'s spin-orbit excitation spectrum, various experimental techniques like THz spectroscopy, IR spectroscopy, and Raman spectroscopy have been used [46]. Warzanowski *et al.* investigated this spectrum and identified the first absorption band as the spin-orbit exciton [47]. Controversies exist, with some suggesting that the featureless spectra could result from magnetic anharmonicity and a breakdown of magnon excitations [48–51]. Nonetheless, α-RuCl$_3$ has demonstrated that any supplementary crystal field effects, such as trigonal or tetragonal distortions, exert negligible influence when contrasted with the prevailing octahedral crystal field [52]. Consequently, despite its comparatively reduced bare spin-orbit coupling (SOC) value, single crystal α-RuCl$_3$ continues to manifest significant SOC-driven effects with an ordered moment characterized by in-plane and out-of-plane anisotropy components [43,44,53,54]. Previous investigations suggest that in-plane anisotropy dominates the bulk crystal of α-RuCl$_3$ and easy-axis anisotropy dominates single-layer samples [55]. Moreover, it has been shown that the in-plane lattice constant
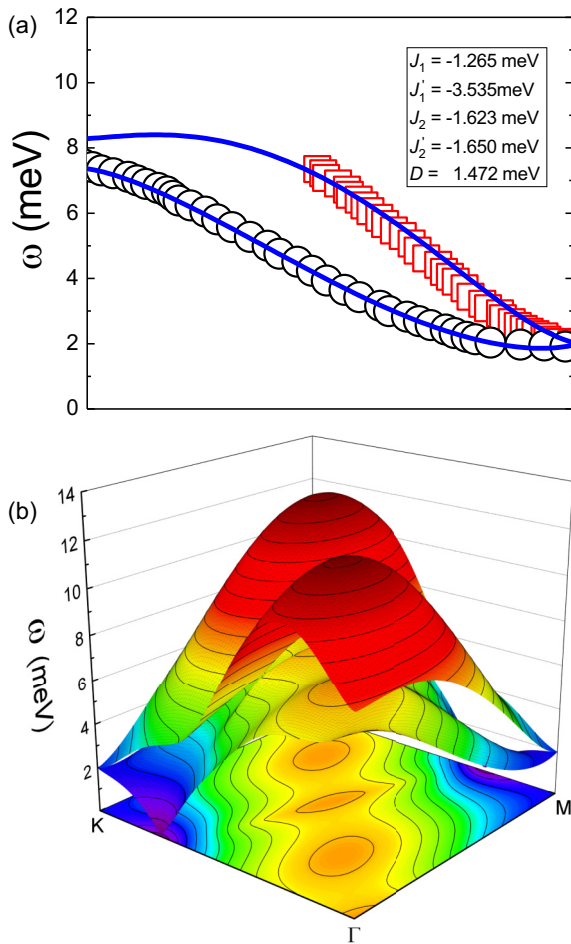
FIG. 7. (a) Comparison of the approximate experimental inelastic neutron scattering data from Ref. [38] to our frustrated model. The black open circles and the red open squares represent the estimated peak position of the lower and upper modes from the experimental data, respectively. The blue line is the frustrated model as it manifests in a zigzag honeycomb lattice through the high-symmetry pathway Γ-M. (b) A 3D plot presenting the frustrated model shows the spin wave throughout the entire Brillouin zone given the parameters needed to reproduce the curves.

expands 3% from 5.99 Å (bulk) to 6.19 Å (monolayer) [56]. Therefore, as layers are removed from a multilayer sample down to a single layer, α-RuCl$_3$ transitions from easy-plane to easy-axis anisotropy [27,55].

Applying a frustrated model with asymmetric superexchange interactions and easy-axis anisotropy, we analyze inelastic neutron scattering data for α-RuCl$_3$ reported in Ref. [38], as shown in Fig. 7. While our model does not incorporate Kitaev-Γ interactions, and the quasiquantum $1/S$ expansion is limited in its ability to capture $S = 1/2$ characteristics fully, we adjusted the exchange parameters to approximate the inelastic neutron scattering data. The primary objective was to investigate whether adjustments to model parameters could present reported behavior, as illustrated in Fig. 7(a). In Fig. 7, the black open circles and the red open squares represent the estimated peak position of the lower and upper modes from the experimental data, respectively. The blue line is the frustrated model as it manifests in a zigzag

honeycomb lattice through the high-symmetry pathway Γ-M. Figure 7(b) presents a three-dimensional (3D) dispersion spanning the Brillouin zone.

Employing a frustrated model with asymmetric exchange interactions and easy-axis anisotropy, we analyzed inelastic neutron scattering data for α-RuCl$_3$. While our model does not encompass Kitaev interactions, this model does approximate the inelastic neutron scattering data [38], aiming to adjust model parameters for a better understanding of the Heisenberg interaction's role within this material. Within this framework, the Holstein-Primakoff expansion facilitates the characterization of spin excitations as potential Dirac magnons, allowing the competition of exchange parameters to encapsulate the competition inherent to the zigzag configuration.

As the honeycomb lattice induces frustration in magnetic configurations, interactions become anisotropic and rely on spins relative to Ru-Ru bonds. Notably, our analysis reconfirms past experiments, emphasizing the prevalence of easy-axis anisotropy in monolayer samples [55]; moreover, our study suggests that a frustrated Heisenberg interaction is an important contributor to shaping the observed spin-wave behavior in α-RuCl$_3$. Overall, this study imparts valuable insights into the lattice's spin dynamics, demonstrating the roles played by competing exchange interactions, asymmetry, and anisotropy in the system's behavior.

IV. CONCLUSIONS

The increasing need for advanced materials in electronic device development has spurred investigations into spintronics and magnonics. These avenues aim to conserve energy while potentially outperforming traditional electronics, resulting in numerous studies [8,16,19,41,45,57,58]. Consequently, comprehending the impact of magnetic interactions on the propagation of spin excitations across diverse lattice configurations becomes paramount for identifying materials amenable to magnon and spin-wave-based applications. This investigation aims to elucidate the influence of various magnetic exchange interactions on the spin dynamics inherent to the zigzag honeycomb lattice.

In this study, we present an analysis of competing nearest-neighbor to next-nearest-neighbor interactions on the spin dynamics of the zigzag honeycomb lattice. Using the exact diagonalization of the Heisenberg Hamiltonian, we determine the spin-wave dynamics and examine the effects of magnetic frustration. Overall, we illustrate that, by building the model term by term, we can directly observe the behavioral contributions from each interaction, how the system changes with anisotropy, and how asymmetric terms transform the system from a nonfrustrated to a frustrated state.

By analyzing geometric frustration, we are able to demonstrate the role that NN and NNN interactions play within an asymmetric honeycomb lattice, show the emergence of direction-dependent Dirac nodes, and postulate that the standard Heisenberg interaction has a notable contribution to the behavior observed in the spin excitation behavior within the high-symmetry pathway. Furthermore, we demonstrate the nature of the spin-wave crossover at the M and K′ symmetry points and discuss the potential for the realization of Dirac magnons.

Additionally, to demonstrate the usefulness of this model, we compare the frustrated Heisenberg model to the inelastic neutron scattering data of α-RuCl$_3$ and show that competing interactions within a Heisenberg framework can produce a similar response to that of Kitaev interactions. This model is not meant to be a definitive study of α-RuCl$_3$, as this is a fit to one data set of the material. However, the fit does show the importance of competing and frustrated interactions in magnetic systems. Furthermore, given the complex nature

observed in this material, this study presents the potential of Dirac physics in α-RuCl$_3$.

ACKNOWLEDGMENTS

[1] P. Souza, T. Ferreto, and R. Calheiros, Maintenance operations on cloud, edge, and IoT environments: Taxonomy, survey, and research challenges, ACM Comput. Surv. **56**, 1 (2024) .

[2] A. Karamchandani, A. Mozo, S. Gómez-Canaval, and A. Pastor, A methodological framework for optimizing the energy consumption of deep neural networks: A case study of a cyber threat detector, Neural Comput. Appl. **36**, 10297 (2024).

[3] S. S. Gill, H. Wu, P. Patros, C. Ottaviani, P. Arora, V. C. Pujol, D. Haunschild, A. K. Parlikad, O. Cetinkaya, H. Lutfiyya, V. Stankovski, R. Li, Y. Ding, J. Qadir, A. Abraham, S. K. Ghosh, H. H. Song, R. Sakellariou, O. Rana, J. J. P. C. Rodrigues, S. S. Kanhere *et al.*, Modern computing: Vision and challenges, Telematics Inf. Rep. **13**, 100116 (2024).

[4] J. Chen, H. Yu, and G. Gubbiotti, Unidirectional spin-wave propagation and devices, J. Phys. D **55**, 123001 (2022).

[5] Y. Sun, F. Meng, C. Lee, A. Soll, H. Zhang, R. Ramesh, J. Yao, Z. Sofer, and J. Orenstein, Dipolar spin wave packet transport in a van der Waals antiferromagnet, Nat. Phys. **20**, 794 (2024).

[6] J. R. Hortensius, D. Afanasiev, M. Matthiesen, R. Leenders, R. Citro, A. V. Kimel, R. V. Mikhaylovskiy, B. A. Ivanov, and A. D. Caviglia, Coherent spin-wave transport in an antiferromagnet, Nat. Phys. **17**, 1001 (2021).

[7] Y. Tokura, M. Kawasaki, and N. Nagaosa, Emergent functions of quantum materials, Nat. Phys. **13**, 1056 (2017).

[8] A. K. Geim and K. S. Novoselov, The rise of graphene, Nat. Mater. **6**, 183 (2007).

[9] K. Vogt, F. Y. Fradin, J. E. Pearson, T. Sebastian, S. D. Bader, B. Hillebrands, A. Hoffmann, and H. Schultheiss, Realization of a spin-wave multiplexer, Nat. Commun. **5**, 3727 (2014).

[10] A. Hirohata, K. Yamada, Y. Nakatani, I.-L. Prejbeanu, B. Diény, P. Pirro, and B. Hillebrands, Review on spintronics: Principles and device applications, J. Magn. Magn. Mater. **509**, 166711 (2020).

[11] R. S. Fishman, J. A. Fernandez-Baca, and T. Rõõm, *Spin-Wave Theory and its Applications to Neutron Scattering and THz Spectroscopy* (Morgan & Claypool, San Rafael, CA, 2018), pp. 2053–2571.

[12] K. S. D. Beach, F. Alet, M. Mambrini, and S. Capponi, SU(N) Heisenberg model on the square lattice: A continuous-N quantum Monte Carlo study, Phys. Rev. B **80**, 184401 (2009).

[13] D. Boyko, A. V. Balatsky, and J. T. Haraldsen, Evolution of magnetic Dirac bosons in a honeycomb lattice, Phys. Rev. B **97**, 014433 (2018).

[14] A. A. Coker, A. Saxena, and J. T. Haraldsen, Effects of exchange distortion and spin rotation in the magnetic kagome lattice, Phys. Rev. B **103**, 054412 (2021).

[15] C. Triola, J.-X. Zhu, A. Migliori, and A. V. Balatsky, Many-body instabilities and mass generation in slow Dirac materials, Phys. Rev. B **92**, 045401 (2015).

[16] J. Fransson, A. M. Black-Schaffer, and A. V. Balatsky, Magnon Dirac materials, Phys. Rev. B **94**, 075401 (2016).

[17] B. Gao, T. Chen, C. Wang, L. Chen, R. Zhong, D. L. Abernathy, D. Xiao, and P. Dai, Spin waves and Dirac magnons in a honeycomb-lattice zigzag antiferromagnet BaNi$_2$(AsO$_4$)$_2$, Phys. Rev. B **104**, 214432 (2021).

[18] K. S. Novoselov, A. K. Geim, S. V. Morozov, D. Jiang, Y. Zhang, S. V. Dubonos, I. V. Grigorieva, and A. A. Firsov, Electric field effect in atomically thin carbon films, Science **306**, 666 (2004).

[19] S. Banerjee, J. Fransson, A. M. Black-Schaffer, H. Ågren, and A. V. Balatsky, Granular superconductor in a honeycomb lattice as a realization of bosonic Dirac material, Phys. Rev. B **93**, 134502 (2016).

[20] J. Chaloupka, G. Jackeli, and G. Khaliullin, Zigzag magnetic order in the iridium oxide Na$_2$IrO$_3$, Phys. Rev. Lett. **110**, 097204 (2013).

[21] J. Chaloupka and G. Khaliullin, Magnetic anisotropy in the Kitaev model systems Na$_2$IrO$_3$ and RuCl$_3$, Phys. Rev. B **94**, 064435 (2016).

[22] Y. Singh and P. Gegenwart, Antiferromagnetic Mott insulating state in single crystals of the honeycomb lattice material Na$_2$IrO$_3$, Phys. Rev. B **82**, 064412 (2010).

[23] J. Cayssol, Introduction to Dirac materials and topological insulators, C. R. Phys. **14**, 760 (2013).

[24] R. Cheng, S. Okamoto, and D. Xiao, Spin Nernst effect of magnons in collinear antiferromagnets, Phys. Rev. Lett. **117**, 217202 (2016).

[25] J. T. Haraldsen, M. Swanson, G. Alvarez, and R. S. Fishman, Spin-wave instabilities and noncollinear magnetic phases of a geometrically frustrated triangular-lattice antiferromagnet, Phys. Rev. Lett. **102**, 237204 (2009).

[26] J. T. Haraldsen and R. S. Fishman, Spin rotation technique for non-collinear magnetic systems: Application to the generalized Villain model, J. Phys.: Condens. Matter **21**, 216001 (2009).

[27] S. Toth and B. Lake, Linear spin wave theory for single-Q incommensurate magnetic structures, J. Phys.: Condens. Matter **27**, 166002 (2015).

[28] A. Auerbach, Hall number of strongly correlated metals, Phys. Rev. Lett. **121**, 066601 (2018).

[29] D. C. Cabra, C. A. Lamas, and H. D. Rosales, Quantum disordered phase on the frustrated honeycomb lattice, Phys. Rev. B **83**, 094506 (2011).

[30] T. Holstein and H. Primakoff, Field dependence of the intrinsic domain magnetization of a ferromagnet, Phys. Rev. **58**, 1098 (1940).

[31] J. B. Fouet, P. Sindzingre, and C. Lhuillier, An investigation of the quantum $J_1 - J_2 - J_3$ model on the honeycomb lattice, Eur. Phys. J. B **20**, 241 (2001).

[32] J. H. P. Colpa, Diagonalization of the quadratic boson Hamiltonian, Physica A (Amsterdam, Neth.) **93**, 327 (1978).

[33] I. O. Ozel, C. A. Belvin, E. Baldini, I. Kimchi, S. Do, K.-Y. Choi, and N. Gedik, Magnetic field-dependent low-energy magnon dynamics in $\alpha - RuCl_3$, Phys. Rev. B **100**, 085108 (2019).

[34] M. M. Nieto and D. R. Truax, Holstein-Primakoff/Bogoliubov transformations and the multiboson system, Fortschr. Phys. **45**, 145 (1997).

[35] P. Tierno, Geometric frustration of colloidal dimers on a honeycomb magnetic lattice, Phys. Rev. Lett. **116**, 038303 (2016).

[36] R. Moessner, Magnets with strong geometric frustration, Can. J. Phys. **79**, 1283 (2001).

[37] M. Swanson, J. T. Haraldsen, and R. S. Fishman, Critical anisotropies of a geometrically frustrated triangular-lattice antiferromagnet, Phys. Rev. B **79**, 184413 (2009).

[38] K. Ran, J. Wang, W. Wang, Z.-Y. Dong, X. Ren, S. Bao, S. Li, Z. Ma, Y. Gan, Y. Zhang, J. T. Park, G. Deng, S. Danilkin, S.-L. Yu, J.-X. Li, and J. Wen, Spin-wave excitations evidencing the Kitaev interaction in single crystalline $\alpha - RuCl_3$, Phys. Rev. Lett. **118**, 107203 (2017).

[39] R. D. Johnson, S. C. Williams, A. A. Haghighirad, J. Singleton, V. Zapf, P. Manuel, I. I. Mazin, Y. Li, H. O. Jeschke, R. Valentí, and R. Coldea, Monoclinic crystal structure of $\alpha - RuCl_3$ and the zigzag antiferromagnetic ground state, Phys. Rev. B **92**, 235119 (2015).

[40] M. Roslova, J. Hunger, G. Bastien, D. Pohl, H. M. Haghighi, A. U. B. Wolter, A. Isaeva, U. Schwarz, B. Rellinghaus, K. Nielsch, B. Büchner, and T. Doert, Detuning the honeycomb of the α-RuCl$_3$ Kitaev Lattice: A case of Cr^{3+} dopant, Inorg. Chem. **58**, 6659 (2019).

[41] A. Banerjee, C. A. Bridges, J.-Q. Yan, A. A. Aczel, L. Li, M. B. Stone, G. E. Granroth, M. D. Lumsden, Y. Yiu, J. Knolle, S. Bhattacharjee, D. L. Kovrizhin, R. Moessner, D. A. Tennant, D. G. Mandrus, and S. E. Nagler, Proximate Kitaev quantum spin liquid behaviour in a honeycomb magnet, Nat. Mater. **15**, 733 (2016).

[42] L. Savary and L. Balents, Quantum spin liquids: A review, Rep. Prog. Phys. **80**, 016502 (2017).

[43] H.-S. Kim, Vijay Shankar V., A. Catuneanu, and H.-Y. Kee, Kitaev magnetism in honeycomb RuCl$_3$ with intermediate spin-orbit coupling, Phys. Rev. B **91**, 241110(R) (2015).

[44] L. J. Sandilands, Y. Tian, A. A. Reijnders, H.-S. Kim, K. W. Plumb, Y.-J. Kim, H.-Y. Kee, and K. S. Burch, Spin-orbit excitations and electronic structure of the putative Kitaev magnet $\alpha - RuCl_3$, Phys. Rev. B **93**, 075144 (2016).

[45] A. K. Bera, S. M. Yusuf, A. Kumar, and C. Ritter, Zigzag antiferromagnetic ground state with anisotropic correlation lengths in the quasi-two-dimensional honeycomb lattice compound Na$_2$Co$_2$TeO$_6$, Phys. Rev. B **95**, 094424 (2017).

[46] A. Loidl, P. Lunkenheimer, and V. Tsurkan, On the proximate Kitaev quantum-spin liquid $\alpha - RuCl_3$: Thermodynamics, excitations and continua, J. Phys.: Condens. Matter **33**, 443004 (2021).

[47] P. Warzanowski, N. Borgwardt, K. Hopfer, J. Attig, T. C. Koethe, P. Becker, V. Tsurkan, A. Loidl, M. Hermanns, P. H. M. van Loosdrecht, and M. Grüninger, Multiple spin-orbit excitons and the electronic structure of $\alpha - RuCl_3$, Phys. Rev. Res. **2**, 042007(R) (2020).

[48] S. M. Winter, A. A. Tsirlin, M. Daghofer, J. van den Brink, Y. Singh, P. Gegenwart, and R. Valentí, Models and materials for generalized Kitaev magnetism, J. Phys.: Condens. Matter **29**, 493002 (2017).

[49] S. M. Winter, K. Riedl, P. A. Maksimov, A. L. Chernyshev, A. Honecker, and R. Valentí, Breakdown of magnons in a strongly spin-orbital coupled magnet, Nat. Commun. **8**, 1152 (2017).

[50] Y. Kubota, H. Tanaka, T. Ono, Y. Narumi, and K. Kindo, Successive magnetic phase transitions in $\alpha - RuCl_3$: XY-like frustrated magnet on the honeycomb lattice, Phys. Rev. B **91**, 094422 (2015).

[51] S. Bachus, D. A. S. Kaib, Y. Tokiwa, A. Jesche, V. Tsurkan, A. Loidl, S. M. Winter, A. A. Tsirlin, R. Valentí, and P. Gegenwart, Thermodynamic perspective on field-induced behavior of $\alpha - RuCl_3$, Phys. Rev. Lett. **125**, 097203 (2020).

[52] J. A. Sears, M. Songvilay, K. W. Plumb, J. P. Clancy, Y. Qiu, Y. Zhao, D. Parshall, and Y.-J. Kim, Magnetic order in $\alpha - RuCl_3$: A honeycomb-lattice quantum magnet with strong spin-orbit coupling, Phys. Rev. B **91**, 144420 (2015).

[53] Q. Luo and H.-Y. Kee, Interplay of magnetic field and trigonal distortion in the honeycomb Γ model: Occurrence of a spin-flop phase, Phys. Rev. B **105**, 174435 (2022).

[54] K. W. Plumb, J. P. Clancy, L. J. Sandilands, V. V. Shankar, Y. F. Hu, K. S. Burch, H.-Y. Kee, and Y.-J. Kim, $\alpha - RuCl_3$: A spin-orbit assisted Mott insulator on a honeycomb lattice, Phys. Rev. B **90**, 041112(R) (2014).

[55] B. Yang, Y. M. Goh, S. H. Sung, G. Ye, S. Biswas, D. A. S. Kaib, R. Dhakal, S. Yan, C. Li, S. Jiang, F. Chen, H. Lei, R. He, R. Valentí, S. M. Winter, R. Hovden, and A. W. Tsen, Magnetic anisotropy reversal driven by structural symmetry-breaking in monolayer α-RuCl3, Nat. Mater. **22**, 50 (2023).

[56] Z. Wang, L. Liu, H. Zheng, M.-Q. Zhao, K. Yang, C. Wang, F. Yang, H. Wu, and C. Gao, Direct observation of the Mottness and p-d orbital hybridization in the epitaxial monolayer α-RuCl3, Nanoscale **14**, 11745 (2022) .

[57] M. Goerbig and G. Montambaux, Dirac fermions in condensed matter and beyond, in *Dirac Matter*, Progress in Mathematical Physics, edited by B. Duplantier, V. Rivasseau, and J. N. Fuchs, Vol. 71 (Birkhäuser, Cham, 2017).

[58] C. Kim, J. Jeong, P. Park, T. Masuda, S. Asai, S. Itoh, H.-S. Kim, A. Wildes, and J.-G. Park, Spin waves in the two-dimensional honeycomb lattice XXZ-type van der Waals antiferromagnet CoPS$_3$, Phys. Rev. B **102**, 184429 (2020).